Longitudinal dependence of open heavy flavor R_{AA} in relativistic heavy-ion collisions

Caio A. G. Prado,[1] Wen-Jing Xing,[1] Shanshan Cao,[2] Guang-You Qin,[1,3] and Xin-Nian Wang[1,3]

[1]*Institute of Particle Physics and Key Laboratory of Quark and Lepton Physics (MOE), Central China Normal University, Wuhan, Hubei 430079, China*

[2]*Cyclotron Institute and Department of Physics and Astronomy, Texas A&M University, College Station, Texas 77843, USA*

[3]*Nuclear Science Division, Lawrence Berkeley National Laboratory, Berkeley, California 94720, USA*

(Received 20 December 2019; revised manuscript received 25 April 2020; accepted 22 May 2020; published 24 June 2020)

Heavy flavor probes are sensitive to the properties of the quark gluon plasma (QGP) produced in relativistic heavy-ion collisions. A huge amount of effort has been devoted to studying different aspects of the heavy-ion collisions using heavy flavor particles. In this work, we study the dynamics of heavy quark transport in the QGP medium using the rapidity dependence of heavy flavor observables. We calculate the nuclear modification of B- and D-meson spectra as well as spectra of leptons from heavy flavor decays in the rapidity range $[-4.0, 4.0]$. We use an implementation of the improved Langevin equation with gluon radiation on top of a $(3 + 1)$-dimensional relativistic viscous hydrodynamical background for several collision setups. We find that the rapidity dependence of the heavy quark modification is determined by the interplay between the smaller size of the medium, which affects the path length of the heavy quarks, and the softer heavy quark initial production spectrum. We compare our results with available experimental data and present predictions for open heavy flavor meson R_{AA} at finite rapidity.

DOI: 10.1103/PhysRevC.101.064907

I. INTRODUCTION

The quark gluon plasma (QGP) produced in relativistic heavy-ion collisions is currently the most perfect fluid in nature [1–5]. Tomographic study of the QGP via jet-medium interaction and jet quenching is one of the most important methods for probing such hot and dense nuclear matter [6,7]. Heavy quarks are particularly valuable probes due to their large masses compared to the QCD scale [8–10]. Since they are mainly created at the very earliest stages of the collisions, the final-state observables from heavy quarks contain cumulative information of the evolution dynamics of the quark gluon plasma.

One of the most common observables pertaining heavy flavor studies is the nuclear modification factor R_{AA}, which compares the yields in nucleus-nucleus collisions with proton-proton collisions, giving information on how the QGP interacts with heavy quarks. In particular, the R_{AA} is important to understand effects that originate from the hot QCD matter produced in the collision and it is commonly associated with parton energy loss through the dense medium. It is defined as the ratio between the particle spectrum in nuclei collisions dN_{AA}/dp_{T}, and the spectrum in pp collisions, $dN_{\mathrm{pp}}/dp_{\mathrm{T}}$ [11]:

$$R_{AA}(p_{\mathrm{T}}, y) = \frac{1}{\mathcal{N}} \frac{dN_{AA}/dp_{\mathrm{T}}dy}{dN_{\mathrm{pp}}/dp_{\mathrm{T}}dy}, \tag{1}$$

in which $\mathcal{N}$ is the average number of binary nucleon-nucleon collisions for a given class of AA collisions.

For the past several years many studies attempted to use R_{AA} to investigate mechanisms of parton transport and energy loss [12–27]. The nuclear modification factor is often used together with other observables in order to obtain stricter constraints on phenomenological models. The anisotropic flow measurements for heavy flavor lead to the so-called $R_{AA} \times v_2$ puzzle [28–31], since many theoretical model calculation underestimate v_2 though they can describe R_{AA}. Further studies on the flow coefficients and event-by-event fluctuations as well as event shape engineering analysis also rely on R_{AA} for an initial constraint of parameters or validation of theoretical models [32–36].

Most studies so far mainly focus on the midrapidity regime. One may also explore the longitudinal dependence of heavy flavor observables, which may put stricter constraints on the currently available models and provide further insight into the dynamics of heavy quarks transport in the QGP medium. Recent studies along this direction focus on the rapidity dependence of the direct flow of D mesons [37–41], though a limited range of rapidity is used. We can also investigate the nuclear modification factor, which is affected mainly by the path length traversed by heavy quarks through the medium and their initial production spectra. In the forward rapidity regime, the medium conditions differ from that at midrapidity, as the system is smaller and thus the path length is shorter. In addition, initial heavy quark production spectra in this regime also differ greatly. Thus, by exploring the behavior of R_{AA} with respect to rapidity one can obtain the picture of QGP medium in a wider range of phase space.

In this study, we investigate the longitudinal dependence of the R_{AA} of heavy flavor mesons (B and D) as well as electrons and muons decayed from these particles. We use

the three-dimensional medium profiles generated from CLVISC viscous hydrodynamics code [42] to construct averaged QGP backgrounds for different collision setups. On top of the hydrodynamics backgrounds, heavy quarks are sampled and allowed to propagate through the medium using a previously developed framework implementing a relativistic Langevin equation with gluon radiation and a hybrid fragmentation plus coalescence model for hadronization [43,44]. Heavy mesons are allowed to decay into electrons and muons. Using the analysis framework developed for DABMOD [32,35] we obtain our final results and compare with currently available experimental data. Predictions are made for different rapidity bins in the range of $-4.0 < y < 4.0$ on the nuclear modification factor of open heavy flavor mesons.

II. ELEMENTS OF THE SIMULATION

In order to simulate the propagation of heavy quarks inside the QGP we use a modified relativistic Langevin equation [43,44], which incorporates two different processes of energy loss inside the medium: quasielastic scattering with light partons in the plasma and gluon radiation induced by multiple scatterings. The Langevin equation can be described by [43,44]:

$$\frac{d\boldsymbol{p}}{dt} = -\eta_D(\boldsymbol{p})\boldsymbol{p} + \boldsymbol{\xi} + \boldsymbol{f}_g, \tag{2}$$

in which the drag coefficient is related to the spatial diffusion coefficient D, the medium temperature T and the heavy quark energy E by the relation $\eta_D = T/(DE)$. In Eq. (2) the last term $\boldsymbol{f}_g$ is added to the original Langevin equation and corresponds to the recoil force exerted on the heavy quarks due to the gluon emission. The other two terms of the equation are the drag force and the thermal force. Here we assume $\boldsymbol{\xi}$ to be independent of the momentum $\boldsymbol{p}$ and satisfies the following correlation function:

$$\langle \xi^i(t)\xi^j(t')\rangle = \kappa\delta^{ij}\delta(t-t'), \tag{3}$$

where κ is the momentum diffusion coefficient and related to the spatial diffusion coefficient as $D = 2T^2/\kappa$. For all the calculations presented in this work, the spatial diffusion coefficient is set as $D(2\pi T) = 8\pi T^3/\hat{q} = 7$, with $\hat{q}/T^3$ being the momentum-independent jet transport parameter. This choice provides the best description of the experimental data that will be shown later. The gluon radiation term in Eq. (2) is calculated from the probability of a gluon emission during a fixed time interval, with the gluon emission spectrum given by the higher twist formalism [45–47]. More details on the implementation of this improved Langevin approach can be found in Refs. [43,44].

The study of longitudinal dependence of observables requires a three-dimensional profile of medium evolution. Therefore, we use the $(3+1)$-dimensional relativistic hydrodynamics code CLVISC [42]. In this work we explore three different collision systems: Au + Au at $\sqrt{s_{NN}} = 200$ GeV, Pb + Pb at $\sqrt{s_{NN}} = 2.76$ TeV, and Pb + Pb at $\sqrt{s_{NN}} = 5.02$ TeV. The hydro simulation is initialized with a smooth initial condition using the TRENTo [48] parametrization that mimics the IP-Glasma [49–51] at initial time $\tau_0 = 0.6$ fm and

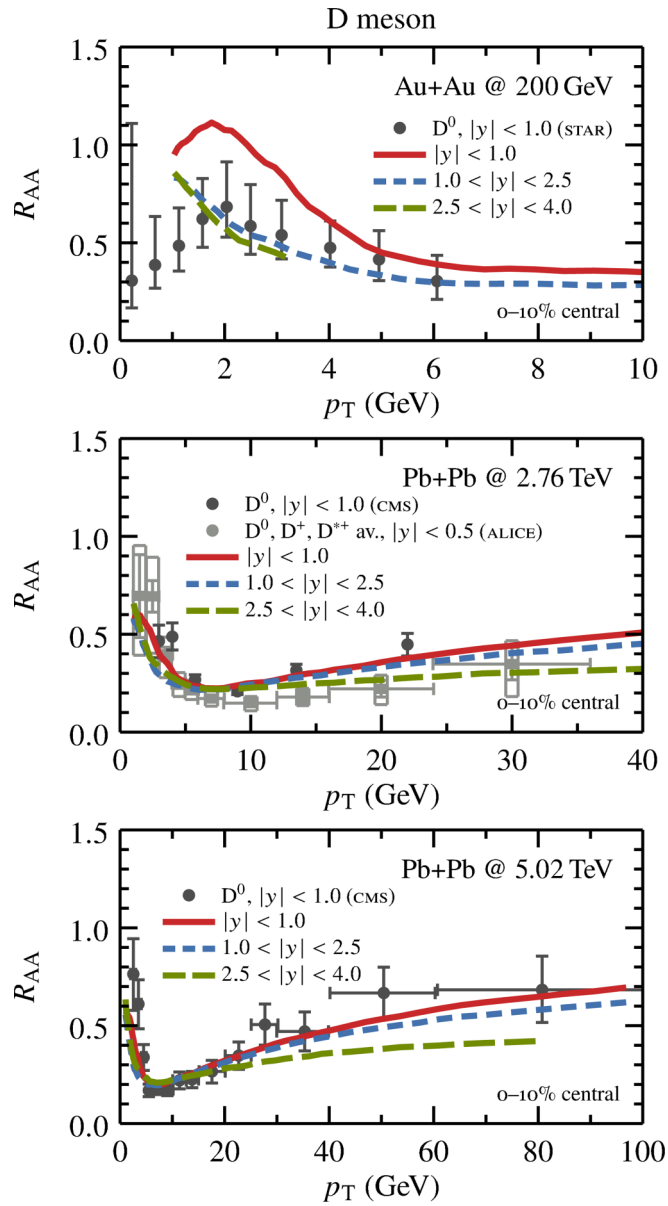

FIG. 1. Nuclear modification factor of D mesons for central collisions in different ranges of rapidity. Midrapidity results are compared with data from STAR [56] (top), ALICE [57], and CMS [58] (middle), and CMS [59] (bottom) at their respective collision energies.

evolve the medium with an EOS described by lattice QCD calculation: s95_PCE, in which the system is partially chemically equilibrated [52]. During the evolution of hydrodynamics we set the shear viscosity as $\eta/s = 0.15$, and the system evolves until the freeze-out temperature $T_{FO} = 137$ MeV is reached. With these setups, the hydrodynamic model is able to provide good descriptions of the soft hadron spectra emitted from the QGP [42].

Heavy quarks are initially sampled within the medium before the hydrodynamic evolution. We determine the initial positions of the heavy quarks production at $\tau = 0$ fm on the transverse plane using the binary collision distribution

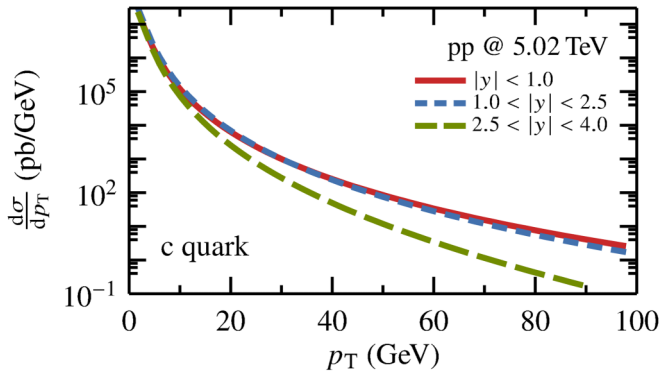

FIG. 2. Heavy flavor production spectra for c quark at different ranges of rapidity for pp at $\sqrt{s} = 5.02$ TeV.

obtained from Monte Carlo Glauber model. The initial momentum distribution of the heavy quarks is calculated using a leading-order perturbative QCD calculation [53] including flavor excitation and pair production processes, as well as nuclear shadowing and antishadowing effects [44,54,55]. Heavy quarks are allowed to propagate freely in the three-dimensional space until $\tau = \tau_0$ when the hydrodynamical evolution begins. They will then transport through the medium and lose energy according to the Langevin equation until their hadronization occurs at the decoupling temperature $T_d = 165$ MeV. The hadronization of heavy quarks uses a hybrid fragmentation and coalescence model [43,44]. Heavy mesons are finally decayed into electrons and muons via PYTHIA.

III. NUMERICAL RESULTS

The results for the D-meson nuclear modification factor are shown in Fig. 1 for collisions of Au + Au at $\sqrt{s_{NN}} = 200$ GeV, Pb + Pb at $\sqrt{s_{NN}} = 2.76$ TeV, and Pb + Pb at $\sqrt{s_{NN}} = 5.02$ TeV. The solid red curves in the plots correspond to the D-meson spectra at midrapidity, which are compared with experimental data. We observe a good agreement with CMS data for both Pb + Pb collisions throughout the whole p_T range. Since CMS data slightly disagree with ALICE, our results overestimate R_{AA} for $\sqrt{s_{NN}} = 2.76$ TeV case in comparison with ALICE data. For the lowest-energy collision of Au + Au at $\sqrt{s_{NN}} = 200$ GeV our results show consistency with data from the STAR experiment for $p_T \geqslant 4$ GeV. At the lower p_T regime a complex interplay of different physical processes is expected to occur. One important effect is the recombination mechanism, which tends to dominate the heavy quark hadronization at this regime.

We also show in Fig. 1 predictions for forward rapidity R_{AA} between $1.0 < |y| < 2.5$ and $2.5 < |y| < 4.0$ rapidity ranges. Lower collision energies reflect in smaller ranges of achievable p_T at large rapidity, as observed in the top panel of the figure for the long-dashed green curve. When increasing the rapidity, we observe a larger suppression at the high-p_T regime, even though the expected medium size in these conditions is smaller. Since R_{AA} not only depends on the path length experienced by the parton inside the medium, but also on the initial production spectra, we expect these two effects

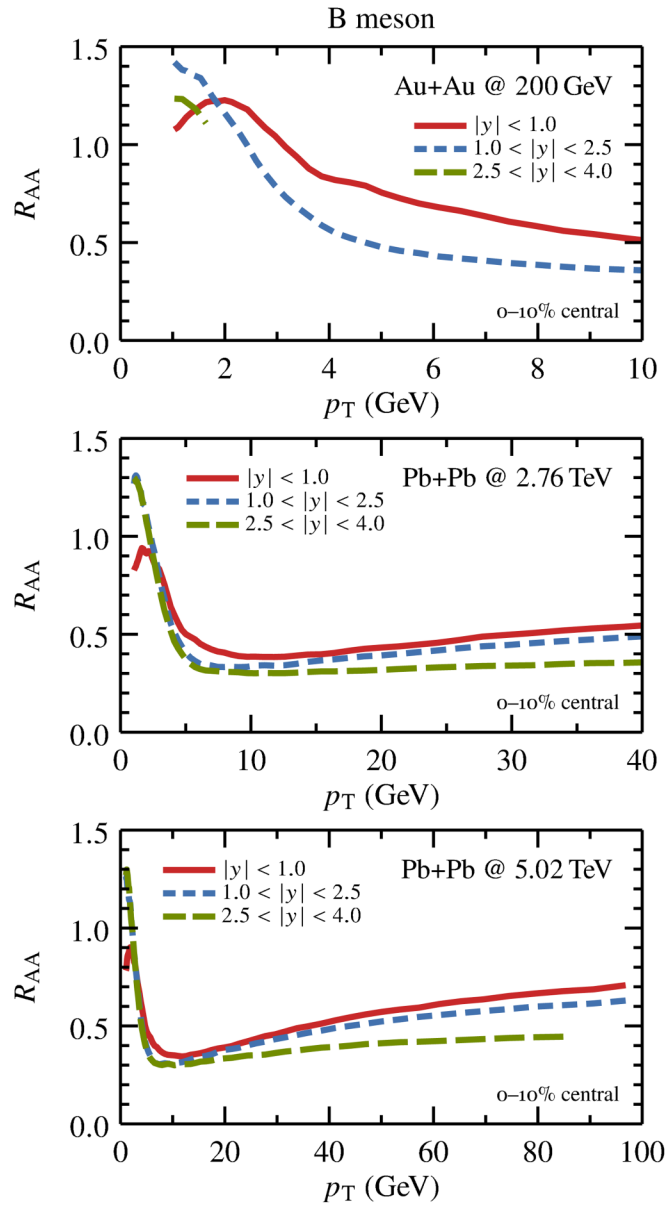

FIG. 3. Nuclear modification factor of B mesons for central collisions in different ranges of rapidity for Au + Au at $\sqrt{s_{NN}} = 200$ GeV (top), Pb + Pb at $\sqrt{s_{NN}} = 2.76$ TeV (middle), and Pb + Pb at $\sqrt{s_{NN}} = 5.02$ TeV (bottom).

to compete in the final result. Here, a stronger effect from the initial heavy quark spectra is observed to dominate in this region of p_T. In Fig. 2 we show effectively how the initial heavy quark spectra becomes steeper for larger rapidity ranges in comparison to the midrapidity range.

Using the same simulation conditions as above, we show in Fig. 3 the results for the B meson R_{AA}. We observe the same trend as the case for D mesons at high p_T, where a larger parton suppression is observed for larger rapidity bins. However, in the case of B mesons we see a clearer separation of the curves at low p_T, together with a more evident crossing for $p_T < 5$ GeV. This suggests that the rapidity dependence at low-p_T regimes may behave differently than

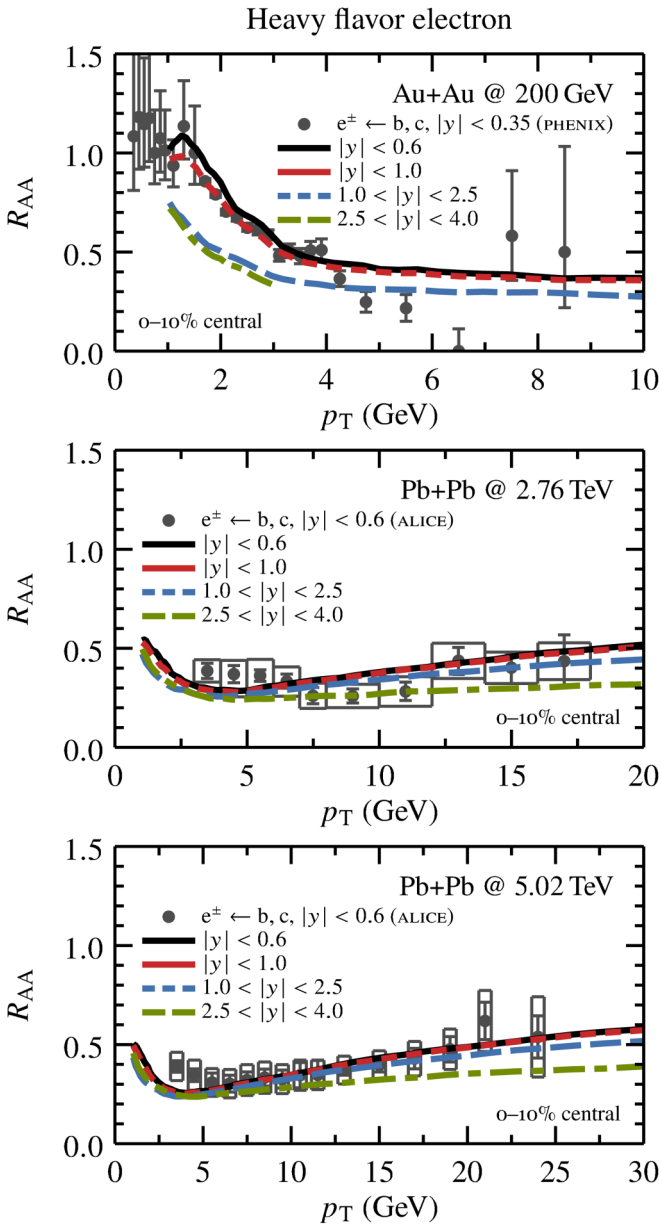

FIG. 4. Nuclear modification factor of heavy flavor electrons for central collisions in different ranges of rapidity. Midrapidity results are compared with data from PHENIX [60] (top), ALICE [61] (middle), and ALICE [62] (bottom) at their respective collision energies.

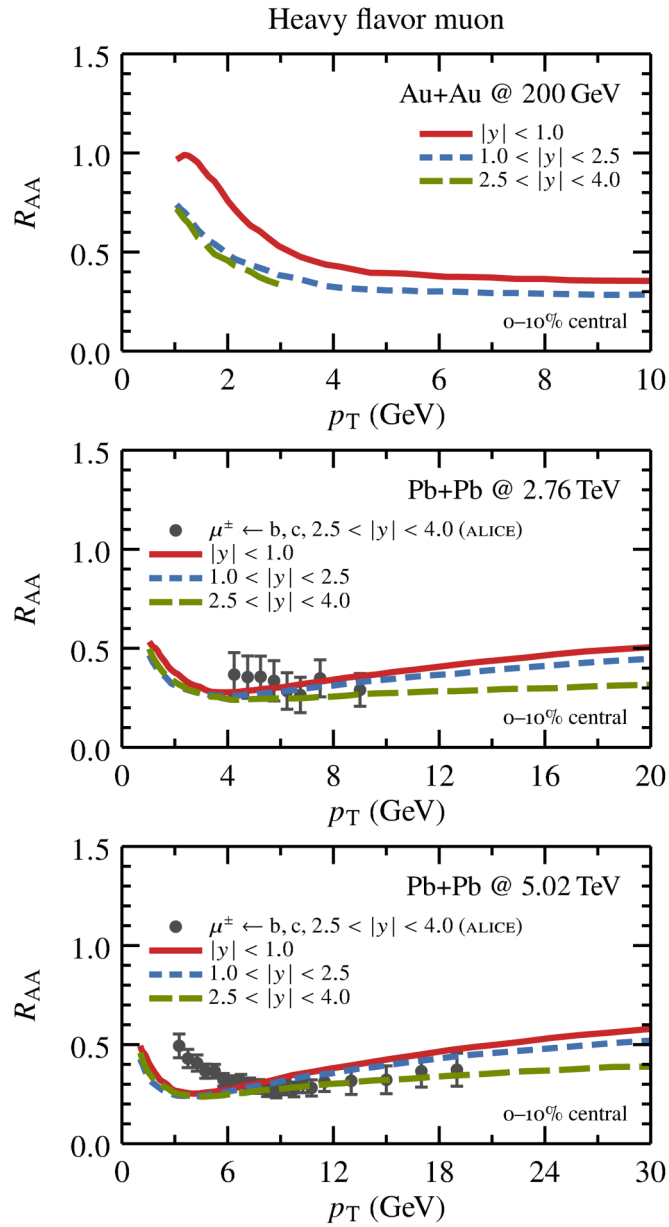

FIG. 5. Nuclear modification factor of heavy flavor muons for central collisions in different ranges of rapidity for Au + Au at $\sqrt{s_{NN}} = 200$ GeV (top), Pb + Pb at $\sqrt{s_{NN}} = 2.76$ TeV (middle), and Pb + Pb at $\sqrt{s_{NN}} = 5.02$ TeV (bottom). Results are compared with experimental data from ALICE [64,65] at forward rapidity.

that at high p_T. Our results are consistent with previous observations on the π^0 nuclear modification factor [63], though the crossing points seem to be at lower p_T in the case of heavy quarks.

After simulation of the heavy meson decays into electrons and muons, we can obtain the nuclear modification factor for these leptons. In Fig. 4 we show heavy flavor electron results. The plots show an additional curve with a smaller rapidity range of $|y| < 0.6$ to be better compared with data from ALICE. The top plot of the figure shows good agreement with data from the PHENIX, even though the rapidity ranges being compared are not exactly the same. In fact, it is expected that around the midrapidity regime, the differences in rapidity have little influence on the results. We also observe a good agreement within error bars for the Pb + Pb collisions at $p_T \gtrsim 5$ GeV. A slight overestimation is observed in the case of Pb + Pb at $\sqrt{s_{NN}} = 2.76$ TeV, which is consistent with the previous result for D mesons in comparison with ALICE in Fig. 1. However, overall agreement are observed at both midrapidities and large rapidities.

In addition to the midrapidity results, Fig. 4 also includes forward rapidity predictions for heavy flavor electrons.

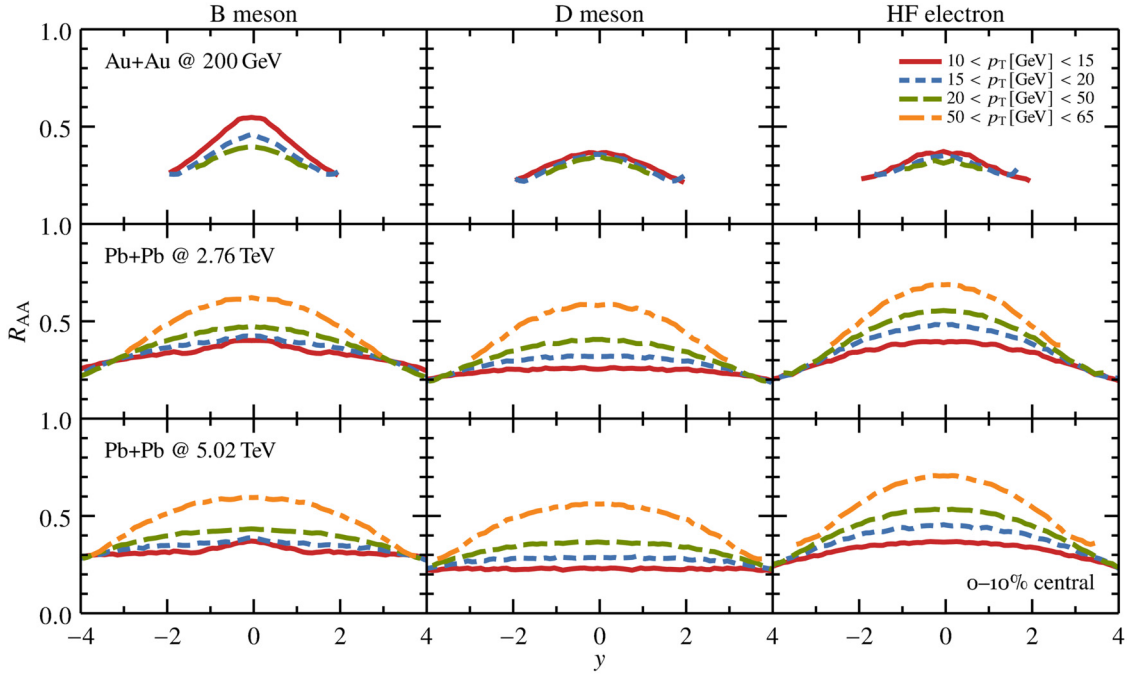

FIG. 6. Nuclear modification factor for selected p_T ranges differential in rapidity for B mesons (left), D mesons (middle), and heavy flavor electrons (right) in central collision systems of Au + Au $\sqrt{s_{NN}} = 200$ GeV (top), Pb + Pb $\sqrt{s_{NN}} = 2.76$ TeV (middle), and Pb + Pb $\sqrt{s_{NN}} = 5.02$ TeV (bottom).

These results reflect what has already been observed for D and B mesons as we see an increase of suppression for large-p_T electrons with large rapidity. We also note the crossing between spectra with different rapidities at low p_T for Pb + Pb collisions.

By simulating the heavy flavor mesons to decay into muons, we obtain the results shown in Fig. 5. We compare our forward rapidity results, showing in long-dashed green curves, with the experimental data for Pb + Pb collisions at both $\sqrt{s_{NN}} = 2.76$ TeV and $\sqrt{s_{NN}} = 5.02$ TeV. The comparison shows good agreement with data for the larger beam energy at high p_T. In particular, by comparing Figs. 4 and 5, we can see that for the high-p_T regime there should be enough resolution to study the rapidity dependence of heavy flavor R_{AA} by comparing theory calculations to data, though the current data error bars are still large. In addition, heavy flavor muon R_{AA} obtained from the simulation falls slightly bellow the experimental data for low p_T as is the case with heavy flavor electrons. Despite that, for $\sqrt{s_{NN}} = 2.76$ TeV collision, our results are consistent with experimental data within error bars, though at this p_T interval, different rapidity bins are also indistinguishable. Finally, the nuclear modification factor for Au + Au collisions are predicted in the top panel.

The plots in Fig. 6 show the rapidity dependence of the nuclear modification factor for different p_T ranges for all the collision systems considered so far. In these plots, comparing different collision energies shows a widening of the R_{AA} curves with increasing energy. In other words, the greater the collision energy, the farther from the midrapidity regime we observe a deviation on the R_{AA} behavior. Another interesting observation is that for two higher-energy Pb + Pb collisions the nuclear modification factor is larger at higher p_T, while for Au + Au collisions R_{AA} is smaller for larger p_T. Again this is due to the initial production spectra of heavy quarks: at the same p_T the spectrum is steeper in lower-energy nuclear collisions.

The above results suggest that measurements of high-p_T particles at finite rapidity may put more constraints on the R_{AA} for better understanding of heavy flavor transport inside the QGP. On the other hand, heavy flavor production in low-p_T region can be further tested in the forward rapidity regime and lower collision energies due to its physical complexity.

IV. CONCLUSIONS

In this work we couple the (3 + 1)-dimensional viscous hydrodynamic medium background modeled by CLVISC with a relativistic Langevin equation-based transport model incorporating both collisional and radiative energy loss of heavy quarks in order to investigate the longitudinal dependence of heavy flavor nuclear modification factor. We verified the consistency between our implementation in a three-dimensional setup and the currently available experimental data at the midrapidity regime for different collision energies. Muon data at finite rapidity were also used to further validate our model. With our simulation, we provided predictions for forward rapidity R_{AA} of heavy flavor mesons and leptons for three different collision energies. We find that the smaller size of the medium at larger rapidity and the steeper initial spectra of heavy quarks at larger rapidity compete with each other. In the end, heavy quarks display small R_{AA} at large rapidity

for large-p_T regime. The nuclear modification behavior at low-p_T regime is more complex due to the interplay of the recombination and other physics effects.

Further studies on the longitudinal dependence of heavy flavor observables are still necessary, in particular, the dependence of flow coefficients coupled with R_{AA} may provide more sensitive constraints on phenomenological models for better understanding of the quark gluon plasma. We hope that the predictions presented in this paper encourage the measurement of finite rapidity observables of heavy flavor final-state particles with higher precision.

ACKNOWLEDGMENTS

This work is supported in part by the Natural Science Foundation of China (NSFC) under Grants No. 11775095, No. 11890711, No. 1861131009, No. 11890714, and No. 11935007, by the China Scholarship Council (CSC) under Grant No. 201906775042, by the US Department of Energy (DOE) under Grants No. DE-AC02-05CH11231 and No. DE-SC0013460, and by the US Natural Science Foundation (NSF) under Grant No. ACI-1550228 within the JETSCAPE Collaboration.

[1] M. Gyulassy and L. McLerran, Nucl. Phys. A **750**, 30 (2005).
[2] E. V. Shuryak, Nucl. Phys. A **750**, 64 (2005).
[3] Star Collaboration, Nucl. Phys. A **757**, 102 (2005).
[4] P. Romatschke and U. Romatschke, Phys. Rev. Lett. **99**, 172301 (2007).
[5] Star Collaboration, Nature (London) **548**, 62 (2017).
[6] X.-N. Wang and M. Gyulassy, Phys. Rev. Lett. **68**, 1480 (1992).
[7] G.-Y. Qin and X.-N. Wang, Int. J. Mod. Phys. E **24**, 1530014 (2015) Jet quenching in high-energy heavy-ion collisions, in *Quark Gluon Plasma 5*, edited by X.-N. Wang (World Scientific, Singapore, 2016), pp. 309–372.
[8] G. D. Moore and D. Teaney, Phys. Rev. C **71**, 064904 (2005).
[9] Wuppertal-Budapest Collaboration, J. High Energy Phys. 09 (2010) 073.
[10] X. Dong, Y.-J. Lee, and R. Rapp, Annu. Rev. Nucl. Part. Sci. **69**, 417 (2019).
[11] M. L. Miller, K. Reygers, S. J. Sanders, and P. Steinberg, Annu. Rev. Nucl. Part. Sci. **57**, 205 (2007).
[12] P. B. Gossiaux, J. Aichelin, T. Gousset, and V. Guiho, J. Phys. G **37**, 094019 (2010).
[13] M. He, R. J. Fries, and R. Rapp, Phys. Rev. C **86**, 014903 (2012).
[14] C. Young, B. Schenke, S. Jeon, and C. Gale, Phys. Rev. C **86**, 034905 (2012).
[15] W. M. Alberico, A. Beraudo, A. De Pace, A. Molinari, M. Monteno, M. Nardi, and F. Prino, Eur. Phys. J. C **71**, 1666 (2011).
[16] J. Uphoff, O. Fochler, Z. Xu, and C. Greiner, Phys. Lett. B **717**, 430 (2012).
[17] M. Nahrgang, J. Aichelin, P. B. Gossiaux, and K. Werner, Phys. Rev. C **90**, 024907 (2014).
[18] S. K. Das, F. Scardina, S. Plumari, and V. Greco, Phys. Rev. C **90**, 044901 (2014).
[19] T. Song, H. Berrehrah, D. Cabrera, W. Cassing, and E. Bratkovskaya, Phys. Rev. C **93**, 034906 (2016).
[20] S. Cao, G.-Y. Qin, and S. A. Bass, Phys. Rev. C **92**, 054909 (2015).
[21] S. Cao, T. Luo, G.-Y. Qin, and X.-N. Wang, Phys. Rev. C **94**, 014909 (2016).
[22] S. Cao, T. Luo, G.-Y. Qin, and X.-N. Wang, Phys. Lett. B **777**, 255 (2018).
[23] S. Cao, A. Majumder, G.-Y. Qin, and C. Shen, Phys. Lett. B **793**, 433 (2019).
[24] S. Y. F. Liu and R. Rapp, Phys. Rev. C **97**, 034918 (2018).
[25] S. Li, C. Wang, X. Yuan, and S. Feng, Phys. Rev. C **98**, 014909 (2018).
[26] W. Ke, Y. Xu, and S. A. Bass, Phys. Rev. C **98**, 064901 (2018).
[27] W.-J. Xing, S. Cao, G.-Y. Qin, and H. Xing, Phys. Lett. B **805**, 135424 (2020).
[28] S. K. Das, M. Ruggieri, F. Scardina, S. Plumari, and V. Greco, J. Phys. G **44**, 095102 (2017).
[29] F. Scardina, S. K. Das, V. Minissale, S. Plumari, and V. Greco, Phys. Rev. C **96**, 044905 (2017).
[30] A. Beraudo, E. Bratkovskaya, P. Braun-Munzinger, S. Cao *et al.*, Nucl. Phys. A **979**, 21 (2018).
[31] S. Cao, G. Coci, S. K. Das, W. Ke *et al.*, Phys. Rev. C **99**, 054907 (2019).
[32] C. A. G. Prado, J. Noronha-Hostler, R. Katz, A. A. P. Suaide, J. Noronha, and M. G. Munhoz, Phys. Rev. C **96**, 064903 (2017).
[33] A. Beraudo, A. De Pace, M. Monteno, M. Nardi, and F. Prino, Eur. Phys. J. C **79**, 494 (2019).
[34] A. Beraudo, A. De Pace, M. Monteno, M. Nardi, and F. Prino, Nucl. Phys. A **982**, 675 (2019).
[35] R. Katz, C. A. G. Prado, J. Noronha-Hostler, J. Noronha, and A. A. P. Suaide, arXiv:1906.10768 [nucl-th].
[36] R. Katz, C. A. G. Prado, J. Noronha-Hostler, and A. A. P. Suaide, arXiv:1907.03308 [nucl-th].
[37] S. K. Das, S. Plumari, S. Chatterjee, J. Alam, F. Scardina, and V. Greco, Phys. Lett. B **768**, 260 (2017).
[38] S. Chatterjee and P. Bożek, Phys. Rev. Lett. **120**, 192301 (2018).
[39] M. Nasim and S. Singha, Phys. Rev. C **97**, 064917 (2018).
[40] Y. Zhang, PoS **345**, 159 (2019).
[41] Star Collaboration, Phys. Rev. Lett. **123**, 162301 (2019).
[42] L.-G. Pang, H. Petersen, and X.-N. Wang, Phys. Rev. C **97**, 064918 (2018).
[43] S. Cao, G.-Y. Qin, and S. A. Bass, Phys. Rev. C **88**, 044907 (2013).
[44] S. Cao, G.-Y. Qin, and S. A. Bass, Phys. Rev. C **92**, 024907 (2015).
[45] X. Guo and X.-N. Wang, Phys. Rev. Lett. **85**, 3591 (2000).
[46] B.-W. Zhang, E. Wang, and X.-N. Wang, Phys. Rev. Lett. **93**, 072301 (2004).
[47] A. Majumder, Phys. Rev. D **85**, 014023 (2012).
[48] J. E. Bernhard, J. S. Moreland, S. A. Bass, J. Liu, and U. Heinz, Phys. Rev. C **94**, 024907 (2016).
[49] B. Schenke, P. Tribedy, and R. Venugopalan, Phys. Rev. Lett. **108**, 252301 (2012).
[50] J. Song, F.-l. Shao, and Z.-t. Liang, Phys. Rev. C **86**, 064903 (2012).
[51] T. Lappi and R. Venugopalan, Phys. Rev. C **74**, 054905 (2006).
[52] P. Huovinen and P. Petreczky, Nucl. Phys. A **837**, 26 (2010).

[53] B. L. Combridge, Nucl. Phys. B **151**, 429 (1979).
[54] Cteq Collaboration, Eur. Phys. J. C **12**, 375 (2000).
[55] K. J. Eskola, H. Paukkunen, and C. A. Salgado, J. High Energy Phys. 04 (2009) 065.
[56] Star Collaboration, Nucl. Phys. A **982**, 659 (2019).
[57] Alice Collaboration, J. High Energy Phys. 03 (2016) 081.
[58] CMS Collaboration, Nuclear modification factor of prompt D^0 in Pb + Pb collisions at $\sqrt{s_{\rm NN}} = 2.76$ TeV, Tech. Rep. CMS-PAS-HIN-15-005, CERN, 2015.
[59] CMS Collaboration, Phys. Lett. B **782**, 474 (2018).
[60] PHENIX Collaboration, Phys. Rev. C **84**, 044905 (2011).
[61] ALICE Collaboration, Phys. Lett. B **771**, 467 (2017).
[62] ALICE Collaboration, HFE R_{AA} with TPC+EMC al in 0–10% Pb + Pb at 5.02 TeV, Fig. ALI-PREL-133360, CERN, 2017.
[63] G.-Y. Qin, J. Ruppert, S. Turbide, C. Gale, C. Nonaka, and S. A. Bass, Phys. Rev. C **76**, 064907 (2007).
[64] ALICE Collaboration, Phys. Rev. Lett. **109**, 112301 (2012).
[65] ALICE Collaboration, HFE R_{AA} with TPC+EMC al and HFM R_{AA} in 0–10% Pb + Pb at 5.02 TeV, Fig. ALI-PREL-133394, CERN, 2017.